Reduction of Edge Reflections in the TLM Model

Ian G. Gosling

Abstract—**In the transmission-line matrix (TLM) method, spurious reflection is encountered at the edge of the mesh. By modeling the infinite region exterior to the mesh by transformation to a finite region and discretization by a second mesh, the magnitude of reflection is much reduced. Numerical results are presented together with an application.**

I. Introduction

THE transmission line matrix (TLM) method is one of the available tools which enable the electromagnetic fields around circuit components and structures to be studied. A full review of the method and comparison with other methods has been given by Hoefer [1], [2]. Other developments are the introduction of the hybrid symmetrical node [3] for a uniform 2-dimensional mesh, which affords some reduction in computer memory requirements, and extensions to mixing of mesh types [4], [5].

Fig. 1 shows how the whole of infinite free space is modeled in reported applications of the TLM method. The finite spatial region I containing the physical structure under study is discretized by a deformed rectangular mesh of link transmission lines and scattering nodes. Because the amplitudes of the wave pulses traveling on the link lines are all kept in computer storage, the mesh can only have a finite number of nodes. The infinite space II exterior to the region under study is not modeled by a mesh at all. Instead, its presence is accounted for by suitably terminating the link transmission lines at the edge of the mesh, which requires a simplifying assumption.

This limitation led early workers to treat only interior boundary value problems such as enclosed waveguides or shielded microstrip [6]. In other problems such as computation of the radiation pattern of antennas, the scattered waves must be allowed to travel outward into free space. The usual simplifying assumption is that terminating the link lines at the edge of the mesh in their own characteristic impedance creates a TEM termination which absorbs incident waves completely. However, this assumption is not exactly true.

When a plane wave is incident on the boundary of the mesh parallel to a mesh axis, Fig. 2(a), the wave can be represented by pulses on only those link lines parallel to the direction of propagation. When these link lines are terminated by an impedance Z_L equal to their own characteristic impedance Z_o, the pulses are completely absorbed in the terminations as required. However, when the wave is incident at some other angle ϕ, Fig. 2(b), the wave must be represented by pulses on all the link lines. The effective load impedance seen by the wave is no longer equal to Z_L but is [7]

$$Z_L \sec \phi \tag{1}$$

where ϕ is the angle of incidence, thereby giving rise to a large unwanted reflection. This reflected wave can be made to vanish for a given value of ϕ by choosing Z_L to make the terminating impedance given by expression (1) equal to Z_o [7]. However, when more than one plane wave, or a nonplane wave, is present, no such termination can cause the reflected wave amplitude to vanish.

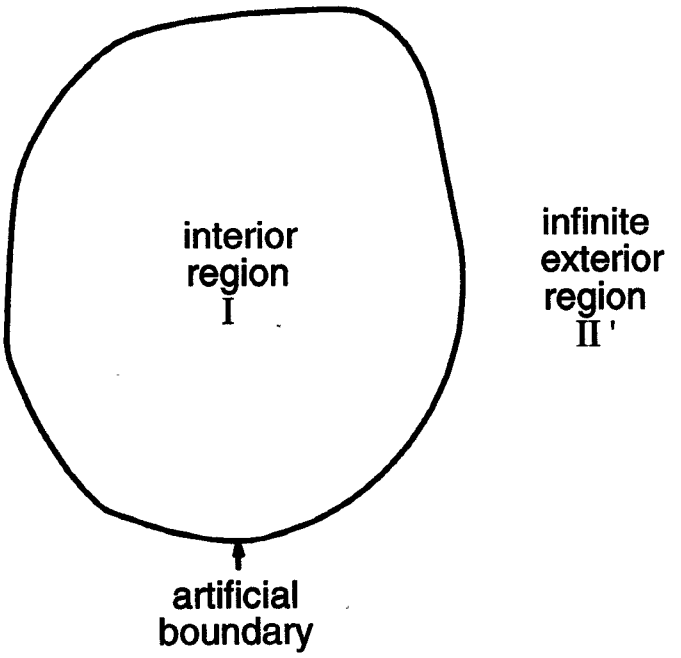

Fig. 1. TLM model of infinite free space.

In another method which keeps the restriction to interior boundary value problems, the mesh is extended to include in the terminating waveguide a physical structure known to act as a matched termination. Alternatively, the terminating waveguide can be modeled using a very large number of nodes so that the initial excitation has not reached the end by the time the computer program is halted [8]. The result achieved is a reflection coefficient of less than 0.03 over a waveguide bandwidth.

A new technique [9], described below, is to model the whole of the infinite region II of Fig. 1 by a transmission-line mesh which is then connected on to the mesh describing region I. In this way, the whole of space is modeled and restriction of the type of problem and the simplifying assumption regarding the edge of the mesh are not needed. It will be seen that

Manuscript received February 10, 1992; revised September 30, 1992.

The author is with Nanyang Technological University, School of Electrical and Electronics Engineering, Nanyang Avenue, Singapore 2263.

IEEE Log Number 9208337.

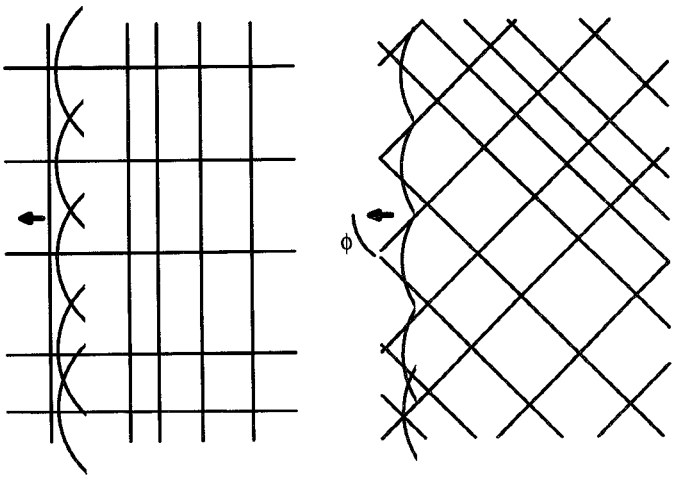

Fig. 2. Reflection from edge of matrix.

a very low reflection coefficient can be achieved, comparing favorably with the results achieved in earlier work. Finally, computed results for an application requiring such a low reflection coefficient will be given.

II. Modeling Infinite Free Space

To develop the infinite free space model, the artificial boundary between regions I and II of Fig. 1 must first be chosen. Region I is modeled directly by a transmission-line mesh, whereas the infinite exterior region II will be transformed, and the transformed region then modeled by another mesh. The boundary should be chosen so that all the physical structure under study and all field source and observation points lie within region I. This is because of the simple way in which the connection between the two matrices is performed: the direction of wave propagation is affected as waves cross the boundary. The mesh spacing in region II also becomes very large near the point at infinity. The model of region II can thus, at present, only be used as an absorber of waves, and not for purposes of prediction of fields in region II. The model of region I retains the full properties of the TLM model.

The model can be used with a variety of types of curvilinear coordinates to describe the two regions. Here, without loss of generality we take the case where region I is modeled by a deformed rectangular mesh. Then the boundary may be naturally be chosen to be cuboid in shape, as this follows the edge of a Cartesian mesh and minimizes the wastage of computer memory. However, other shapes may be chosen, see below.

The infinite region II is now transformed conformally to the finite region II $'$ of Fig. 3. The transformation is chosen so that the boundary between regions I and II maps to itself, and the point at infinity maps to the origin (which should lie within region I). To accomplish this, we must first formulate the TLM method in arbitrary orthogonal curvilinear coordinates [10]. We take (x, y, z) to be Cartesian coordinates in region II and (ξ, υ, ζ) to be curvilinear coordinates in region II $'$. The

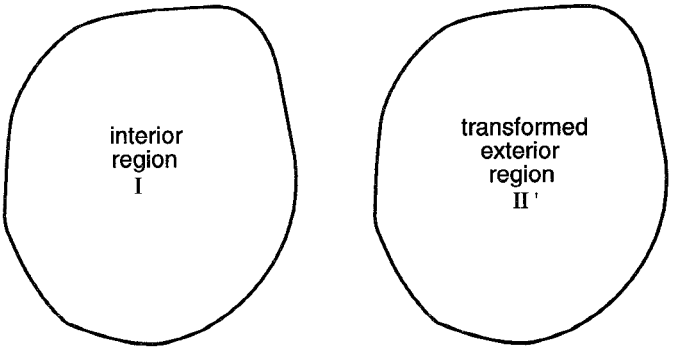

Fig. 3. Transformation of Fig. 1 to two identical finite regions.

x-components of the two Maxwell equations

$$\operatorname{curl} \boldsymbol{H} = \epsilon \partial \boldsymbol{E}/\partial t + \sigma \boldsymbol{E} \tag{2a}$$

$$\operatorname{curl} \boldsymbol{E} = -\mu \partial \boldsymbol{H}/\partial t, \tag{2b}$$

are

$$\partial/\partial \upsilon(h_\zeta H_\zeta) - \partial/\partial \zeta(h_\upsilon H_\upsilon) = h_\upsilon h_\zeta \epsilon \partial E_\xi/\partial t + h_\upsilon h_\zeta \sigma E_\xi \tag{3a}$$

$$\partial/\partial \upsilon(h_\zeta E_\zeta) - \partial/\partial \zeta(h_\upsilon E_\upsilon) = -h_\upsilon h_\zeta \mu \partial H_\xi/\partial t \tag{3b}$$

where $h_{\xi,\upsilon,\zeta}$ are the metrics in the three transformed local coordinate axes. In the TLM model, we discretize these equations at the coordinates of a mesh node by introducing nodal voltages $V_{\xi,\upsilon,\zeta}$ and nodal loop currents $I_{\xi,\upsilon,\zeta}$. Following the procedure of Section II of [11], when the voltages and currents are given by

$$\begin{aligned} E_\xi &\equiv V_\xi/h_\xi a, \\ H_\upsilon &\equiv I_\zeta/h_\upsilon b, \\ H_\zeta &\equiv -I_\upsilon/h_\zeta c, \\ \epsilon &\equiv C_\xi h_\xi a/h_\upsilon b h_\zeta c, \\ \sigma &\equiv G_\xi h_\xi a/h_\upsilon b h_\zeta c \end{aligned} \tag{4}$$

in (3a), and

$$\begin{aligned} H_\xi &\equiv -I_\xi/h_\xi a, \\ E_\upsilon &\equiv V_\upsilon/h_\upsilon b, \\ E_\zeta &\equiv V_\zeta/h_\zeta c, \\ \mu &\equiv L_\xi h_\xi a/h_\upsilon b h_\zeta c \end{aligned} \tag{5}$$

in (3b), then (3) reduces to Kirchoff's current and voltage laws at each node. Similarly for the other field components. Here $C_{\xi,\upsilon,\zeta}$ are the total shunt capacitances at the shunt connections in the node, $G_{\xi,\upsilon,\zeta}$ are conductances placed to give loss, and $L_{\xi,\upsilon,\zeta}$ are the total inductances in the series connections. a, b, c are the local cell dimensions of the mesh in region II$'$.

The characteristic impedances of the link transmission lines and stubs at each node of the mesh are now chosen so that the total capacitance and inductance they present at the node are equal to $C_{\xi,\upsilon,\zeta}$ and $L_{\xi,\upsilon,\zeta}$, respectively. The symmetrical condensed node formulation [11] has twelve link transmission lines connected to each node, having characteristic impedance

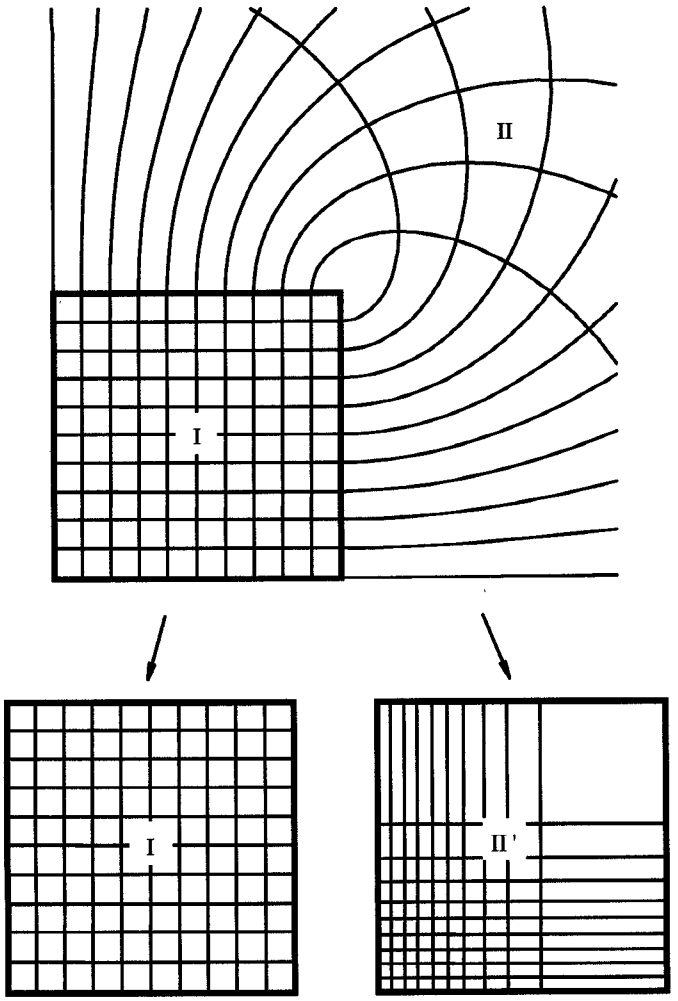

Fig. 4. Matrices used when the boundary is a cube.

equal to Z_o, and the balance of capacitance and inductance is represented by six stubs of characteristic impedances $Z_o/Y_{s\xi,sv,s\zeta}$ and $Z_oZ_{s\xi,sv,s\zeta}$ where

$$\begin{aligned} Y_{s\xi} &= 4(\epsilon_r h_\xi a h_v b/h_\zeta ch - 1) \\ Y_{sv} &= 4(\epsilon_r h_v b h_\zeta c/h_\xi ah - 1) \\ Y_{s\zeta} &= 4(\epsilon_r h_\zeta c h_\xi a/h_v bh - 1) \\ Z_{s\xi} &= 4(\mu_r h_\xi a h_v b/h_\zeta ch - 1) \\ Z_{sv} &= 4(\mu_r h_v b h_\zeta c/h_\xi ah - 1) \\ Z_{s\zeta} &= 4(\mu_r h_\zeta c h_\xi a/h_v bh - 1). \end{aligned} \tag{6}$$

where h is a constant chosen to make the right-hand side nonnegative at all nodes.

Alternatively, in the hybrid condensed node formulation [3], the link transmission lines have characteristic impedances chosen to account for all the inductance, given by $Z_o/Y'_{\xi,v,\zeta}$ where

$$\begin{aligned} Y'_\xi &= h_\xi ah/\mu_r h_v bh_\zeta c \\ Y'_v &= h_v bh/\mu_r h_\zeta ch_\xi a \\ Y'_\zeta &= h_\zeta ch/\mu_r h_\xi ah_v b. \end{aligned} \tag{7}$$

Only three stubs are required, and they account for the balance of capacitance. Their characteristic impedances are

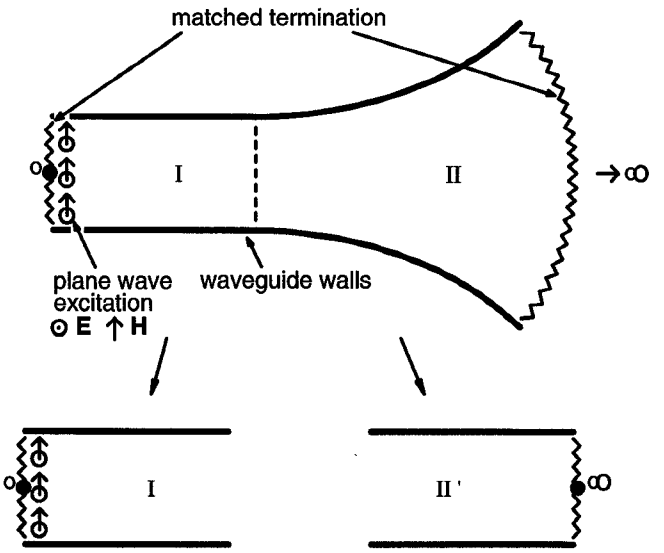

Fig. 5. Waveguide and horn used in numerical experiment.

$Zo/Y'_{s\xi,sv,s\zeta}$ where

$$\begin{aligned} Y'_{s\xi} &= 4\epsilon_r h_v bh_\zeta c/h_\xi ah - 2(Y'_v + Y'_\zeta) \\ Y'_{sv} &= 4\epsilon_r h_\zeta ch_\xi a/h_v bh - 2(Y'_\zeta + Y'_\xi) \\ Y'_{s\zeta} &= 4\epsilon_r h_\xi ah_v b/h_\zeta ch - 2(Y'_\xi + Y'_v). \end{aligned} \tag{8}$$

h is chosen as before and can be chosen larger than the maximum value for the symmetrical condensed node, thus, reducing the computation time required.

To complete the development of the TLM method, the line and stub impedances are inserted in the scattering matrix at each node, given by [12] for the symmetrical condensed node and by [3] for the hybrid condensed node. The scattering matrix of the node representing the point at infinity is set to the zero matrix.

For the hybrid condensed node formulation, it will be seen from (7) that even with a uniform node spacing, the inductance varies from one node to another because the metrics are functions of position, and thus the characteristic impedance of the link lines connected to adjacent nodes may be different. Scattering at the junction of link lines halfway between the nodes must therefore be included, which offsets the reduction in the amount of computation expected with this type of node. The scattering matrix at the junction of cells n and $n+1$ is, in terms of voltages,

$$\frac{1}{Y_n + Y_{n+1}} \begin{bmatrix} Y_n - Y_{n+1} & 2Y_{n+1} \\ 2Y_n & Y_{n+1} - Y_n \end{bmatrix}. \tag{9}$$

The time step in real time is

$$\Delta t = h/2c_o \tag{10}$$

where c_o is the speed of light in vacuum.

We must also remember to implement connection between regions I and II of Fig. 1. This is the same as connecting region I to the transformed region II′ of Fig. 3. To accomplish this, we note that regions I and II′ share an identical outer boundary. The transformation should be chosen such that the ends of the link transmission lines at the edge of the mesh modeling

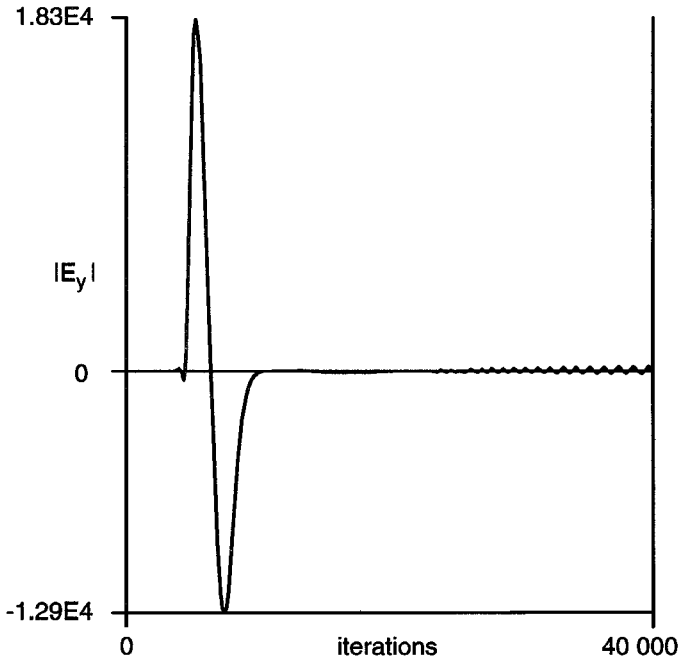

Fig. 6. Incident and reflected wave pulses.

region I automatically coincide in position with those at the edge of region II′. The algorithm to implement connection is then a simple copy instruction from one mesh to the other.

III. Cubic Boundary

We now apply the method to particular cases. We first take the boundary separating the interior finite region I and the exterior infinite region II to be a cube. (The general case of a cuboid can be transformed to a cube by linear scaling along one or two axes.) The appropriate transformation from region II to region II′ is

$$\xi + j\upsilon = Z^{-1}\left(\frac{4}{\pi}(x + jy)\right), \qquad 0 \le x, y \le 1$$
$$\zeta = z \tag{11}$$

where Z is the lemniscatic Weierstrass zeta-function, which is defined in one quadrant, and similarly by symmetry for the other quadrants $-1 \le x, y \le 0$. This transforms only two of the three dimensions, and can thus only be applied to a restricted class of problems. The metrics are given by

$$h_\xi = h_\upsilon = |\mathcal{P}(\xi + j\upsilon)|$$
$$h_\zeta = 1 \tag{12}$$

where $\mathcal{P}$ is the Weierstrass $\mathcal{P}$-function. Weierstrass functions may be evaluated using the first few terms of the power series of [13]. The effect of the transformation is shown in Fig. 4. It will be seen that the cell just outside the boundary differs in size considerably from that just inside, that the cell sizes in region II′ are not uniform, and that space is distorted around the corner of the cube. These are disadvantages which may limit the usefulness of this transformation.

To test the method, a nondispersive rectangular waveguide was formed by placing electric walls normal to the E-plane, and magnetic walls normal to the H-plane, as shown in Fig. 5. The waveguide was continued outside the cubic boundary following the directions of the link lines of the mesh to form an infinitely long horn antenna. The waveguide could be swiveled around to investigate reflection for different values of ϕ. Both ends were terminated by a flat reflecting sheet of zero reflection coefficient. Excitation was by a Gaussian pulse plane wavefront at the end nearest the origin, Fig. 6, [7]. It is limited in its time extent, allowing the incident pulse to be differentiated from any reflected pulses. It also has a bandlimited power spectrum. This allows reduction in pulse dispersion due to velocity error on the mesh.

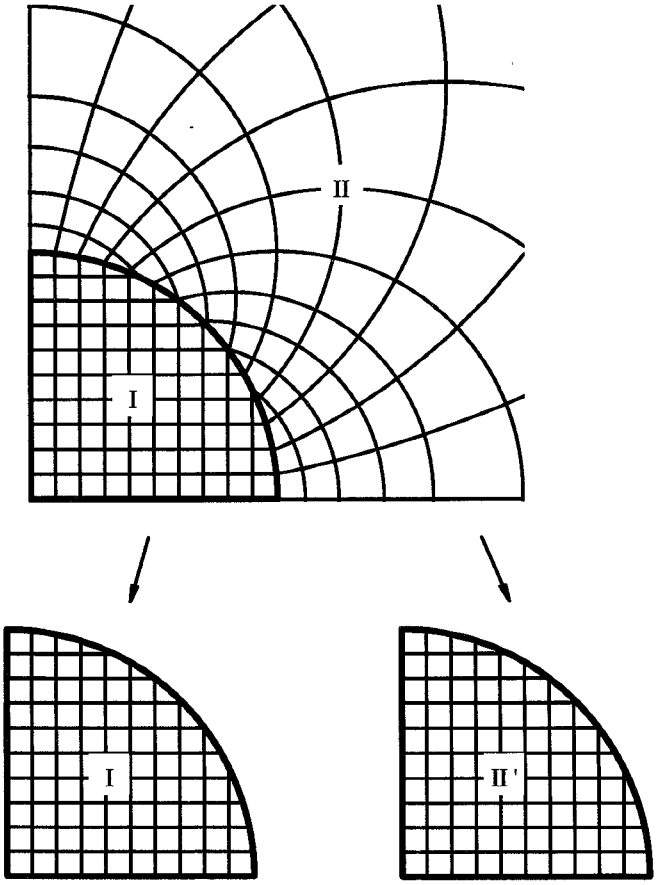

Fig. 7. Matrices for a spherical boundary.

When the node spacing in the finite interior region I was 1 length unit, and the half-side of the cube was 120.5 units, the corresponding node spacings in the transformed region II′ varied considerably along the side of the cube, between 0.46 and 22.6 units. Because of this wide variation, the symmetrical condensed node was chosen because it was found in some cases to have a lower sensitivity to differences in node spacing between adjacent nodes, as demonstrated in the results of Section VI below. Then h must be small, in this case 0.02 units, implying a small time step and a long computation time. Some adjustment of the node spacing in region I to vary between 0.1 and 1 unit gave a slightly better value of h of 0.03 units. The spectral bandwidth of the exciting pulse was kept below 0.05 times the cutoff frequency on the mesh.

TABLE I
RESULTS FOR THE SPHERICAL BOUNDARY

node type	waveguide orientation	h	refl. coeff. with TEM boundary	refl. coeff. with exterior region
symm. cond.	0°	0.67	0	2×10-6 [9]
	45°	0.28	0.172	0.005 [9]
hybrid cond.	0°	0.99	0	0.0013
	45°	0.50	0.172	0.024

The E_y field component was observed at a point midway between the origin and the boundary of the cube. When the waveguide was directed from the origin along an axis of the mesh, the reflection coefficient was 0.008 or -41 dB, Fig. 6, a good result which compares well with the results of previous work referred to above. A return signal can be seen at a very high number of iterations, higher than would normally be used in solving an application problem. Another run was performed with the waveguide oriented at an angle of 45° to the x-axis, and lying in the x-y plane The result should be expected to be worst here because of high dispersion in the mesh for propagation in this direction, and because of the sharp change in node spacing at the corner of the cube, through which the waveguide was chosen to pass. h had to be reduced to 8×10^{-4}, and a reflection coefficient of 0.78 was computed, with the reflected pulse arriving back at the origin after 29 000 iterations. This poor result with an extraordinarily long run time is because of the large distortion of space near the corners of the cube.

IV. SPHERICAL BOUNDARY

A spherical boundary between regions I and II is another possibility, Fig. 7. With the spherical shape, if a whole cubic mesh is stored in computer memory, then only about half the volume is inside the inscribed sphere, so that half the memory is unused. This inefficiency may be remedied by storing only the data for those nodes lying inside the sphere. The appropriate transformation from region II to region II′ is the vector reciprocal

$$(\xi, \upsilon, \zeta) = (x/r^2, y/r^2, z/r^2), \qquad r^2 = x^2 + y^2 + z^2. \tag{13}$$

The metrics are given by

$$h_\xi = h_\upsilon = h_\zeta = r^2. \tag{14}$$

Now, not only does the boundary transform to itself, but each point on the boundary also transforms to itself, removing the difficulty of variation of node spacing encountered with the cubic boundary. Because the transformation is conformal, the angle of incidence to the sphere of the link transmission lines just inside the surface of the sphere is the same as the angle of incidence of those just outside. It will be seen from Fig. 7(a) that this causes the direction of propagation along the link lines in real space to change sharply across the spherical boundary, especially around 45° latitude. However, if we ensure that the entire object or device to be modeled is contained within the sphere, then the exterior region is only used as an absorber; one is not interested in the exact values of the fields here. It will also be seen from the figure that the dimensions of those cells just inside the surface of the sphere are different from their neighbors. This must be accounted for by modifying the characteristic impedances of the stubs for these nodes by substituting the local cell dimensions into (6).

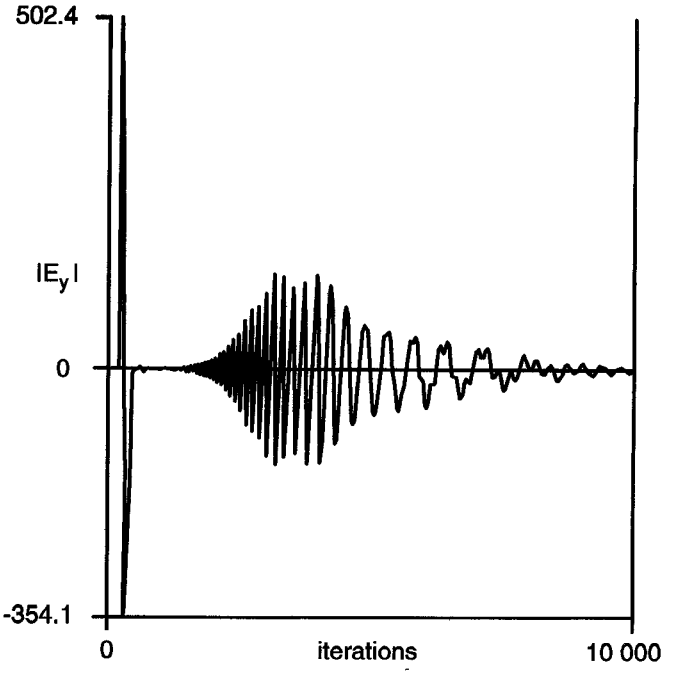

Fig. 8. Reflected signal for infinite exterior region.

The same nondispersive waveguide was modeled using the spherical boundary. The node spacing was 1 length unit and the radius of the sphere was 120.5 units. The hybrid condensed node was used. Waveguide orientations were chosen again firstly along one mesh and, secondly, at an angle of 45° to one axis, where pulse dispersion and the change of direction of link lines should give a worse result. The field observation point was midway between the origin and the surface of the sphere.

The value of h and the computed reflection coefficient are shown in Table I together with those for the spherical condensed node from [9]. In some cases, the reflected waves were buried in the numerical noise, so the figures in the table are accurate to between one and two significant figures. As in the case of the cubic boundary, a high frequency return signal became apparent at a large number of iterations, again a larger number than would be used in a normal application. The value of h for the hybrid condensed node is about half that

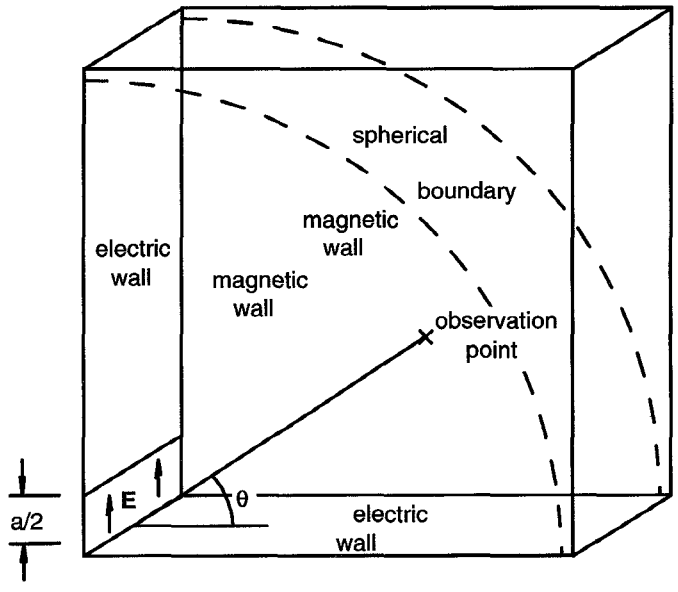

Fig. 9. TLM model of diffraction through a narrow slit.

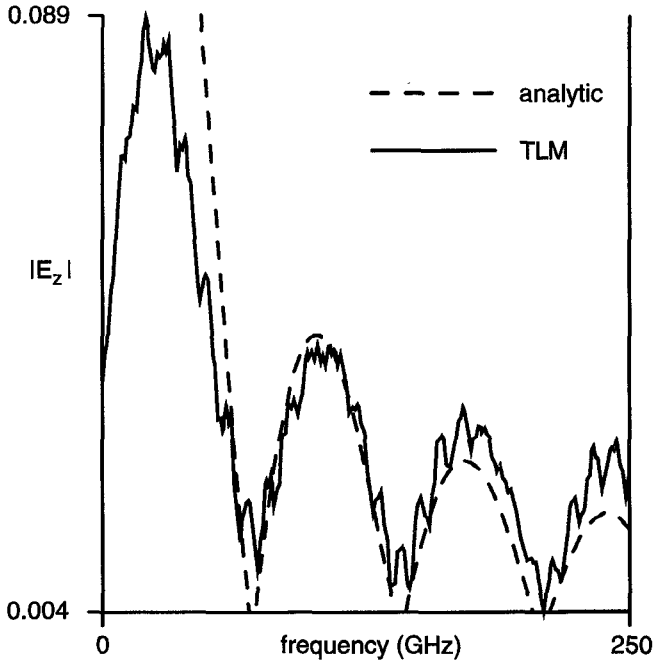

Fig. 10. Spectrum of field diffracted through a slit, matrix edge matched.

for the symmetrical condensed node, so that the execution time of the program is about half for the hybrid condensed node formulation. For comparison, the reflection coefficient for a TEM boundary with no exterior region is included, computed from the load impedance in (1).

When the waveguide was pointed along an axis of the mesh, an extremely low reflection coefficient was achieved in the case of the symmetrical condensed node, an excellent result. When the waveguide was pointed at 45° to one of the axes of the mesh, and for the hybrid condensed node, the reflection coefficient was higher, but still very small, around 0.0013 to 0.024 or −58 dB to −32 dB. This compares well with the results of other methods noted above [8], [9], where reflection coefficients of as low as 0.03 were reported, and is much less than the value for the TEM boundary alone. Surprisingly, the low result is achieved despite the abrupt change of direction of the link lines at the surface of the sphere. This may be because the wavefront still propagates properly along the horn, although the contributing wavelets along the link lines become interchanged as they cross the spherical surface.

V. Limiting the Size of the Exterior Region

If only a part of the region II of Fig. 1 needs to be modeled, then computer storage and time requirements are reduced. To study this aspect, the horn described in Section IV above was truncated by bringing the plane of match-terminated link transmission lines, Fig. 5, closer to the spherical boundary. Computer storage is not required to model the space beyond the plane. When the program was run, the incident pulse was followed in time by the small pulse reflected from the boundary, then by a large undispersed pulse reflected from the terminating plane. This suggests that the reflection coefficient reported above is due chiefly to the abrupt change in direction of link transmission lines at the boundary.

As the position of the plane was moved from the spherical boundary outwards towards infinity, the large reflected pulse returned after a larger number of iterations, as would be expected, but grew in amplitude. When the position of the plane approached the node representing the point at infinity, the large reflected pulse ceased to grow in amplitude and became substantially dispersed. Fig. 8 shows the reflected pulse in this limiting case.

From these results, it is recommended that for a small number of iterations of the method, the computer storage for the mesh modeling space outside a certain radius from the origin may be released. That radius is determined by the number of iterations taken for the large reflected pulse to reach the field observation point. Alternatively, if the whole of infinite space is to be modeled, the number of iterations must be limited so that the dispersed pulse has not yet returned.

VI. Application: Diffraction

An example application is the simulation of the far field for diffraction through a long narrow slit of width a excited by a uniform electric field across the slit. The analytical solution to this is well known and is

$$E = k \operatorname{sinc}(\beta a \sin \theta) \tag{15}$$

where k is a constant, β is the free-space propagation constant, θ is the scattering angle, and E is the observed electric field amplitude. This is a difficult problem for the TLM method as the node spacing must be small so that the zeros of the sinc function fall below the cutoff frequency of the mesh [2]. This means that the mesh must contain a large number of nodes, increasing computer storage and run time requirements substantially. In addition, with a far field observation point,

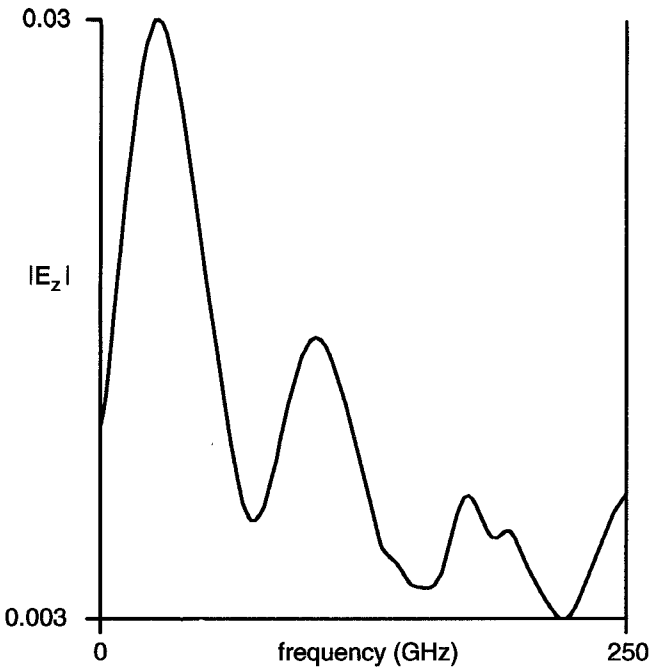

Fig. 11. Diffracted field, spherical boundary.

any reflection from the edge of the TLM mesh may interfere with the diffracted field, causing errors in the result.

The TLM model is shown in Fig. 9. Advantage is taken of symmetry to reduce the size of the problem in the long axis of the slit by introducing a pair of magnetic image planes, and in its short axis by introducing an electric image plane. The slit width was $a = 6.0$ mm, the node spacing 0.3 mm, and the field observation point distant 60.45 mm from the slit at $\theta = \pi/4$. This required a large mesh of $201 \times 3 \times 201$ nodes in (x, y, z) directions, respectively. The simulation was limited to 2047 iterations to give good frequency accuracy but truncated before the expected dispersed reflected pulse had any effect. From (15), the zeros of the diffracted field are expected to fall at multiples of 70.7 GHz. With the edge of the mesh match-terminated, the spectrum of the simulated field is compared with the analytic result in Fig. 10. The symmetrical condensed node and hybrid condensed node formulations gave identical results. The zeros do fall where expected, but the response has a short-period ripple superposed, typical of an interfering reflected signal such as the reflection from the edge of the mesh. The discrepancy in the low frequency response is attributed to time series truncation error.

When the method described in this paper is applied, with a surrounding spherical boundary, Fig. 11, the ripple is absent in the result for the symmetrical condensed node, corresponding to the reduced reflection from the edge of the mesh. The result for the hybrid condensed node did not show a strongly enhanced behavior. This is attributed to spurious scattering at the spherical boundary where the local cell dimensions vary from the 0.3 mm cube.

VII. Conclusion and Recommendations

This paper has described a method of modeling the infinite space outside the region under study in the TLM method. This can be done by dividing space with a boundary surface and using a transformation and two transmission-line matrices instead of one. A cubic boundary, used with the Weierstrass transformation, gives quite poor results. However, when a spherical boundary and the reciprocal transformation are used, the amplitude of reflections at the edge of the mesh is reduced to between 2×10^{-6} and 0.024, depending on the position of the reflecting point relative to the axes of the mesh, and on which node formulation is used. These results compare well with those of other methods, where a reflection coefficient as low as 0.03 has been reported. A cubic mesh in Cartesian coordinates has been used in this work. It would be expected that a lower reflection coefficient could be achieved if a mesh based on spherical polar coordinates were used with a spherical boundary, as this eliminates the abrupt change in direction of the link transmission lines at the boundary. This would be suitable when the physical structure of the device under study lends itself to description in spherical coordinates.

When the mesh describing the infinite region outside the boundary is limited in size by not modeling space beyond a certain distance from the origin, or when a large number of iterations is used, a large reflected signal is observed. This number of iterations is normally larger than that required for a certain level of truncation error in a given application. It is recommended that the number of iterations required to limit truncation error be used as a guide to how much of the mesh may safely be omitted.

References

[1] W. J. R. Hoefer, "The transmission-line matrix method—Theory and applications." *IEEE Trans. Microwave Theory Tech.,* vol. MTT-33, pp. 882–893, Oct. 1985.

[2] T. Itoh, Ed., "The transmission line matrix (TLM) method," *Numerical Techniques for Microwave and Millimetre-Wave Passive Structure,* ch. 8. New York: Wiley, 1989.

[3] R. Scaramuzza and A. J. Lowery, "Hybrid symmetrical condensed node for the TLM method," *Elec. Lett.,* vol. 26, pp. 1947–1949, Nov. 8, 1990.

[4] L. J. Herring and C. Christopoulos, "Multigrid transmission-line modeling method for solving electromagnetic field problems," *Elec. Lett.,* vol. 27, pp. 1794–1795, Sept. 26, 1991.

[5] D. P. Johns, J. Wlodarcyzk, and A. Malik, "New TLM models for thin structures," in *Proc. Int. Conf. Comput. Electromagnetics,* London, Dec. 1991, pp. 335–338.

[6] J. E. Sitch and P. B. Johns, "Transmission-line matrix analysis of continuous waveguiding structures using stepped-impedance cavities," *Microwaves, Optics, Acoustics,* vol. 1, pp. 181–184, Sept. 1977.

[7] N. R. S. Simons and E. Bridges, "Method for modeling free space boundaries in TLM situations," *Elec. Lett.,* vol. 26, pp. 453–455, Mar. 20, 1990.

[8] Eswarrapa *et al.*, "Transmission line matrix modeling of dispersive wideband absorbing boundaries with time-domain diakoptics for S-parameter extraction," *IEEE Trans. Microwave Theory Tech.,* vol. 38, pp. 379–386, Apr. 1990.

[9] I. G. Gosling, "Modeling of absorptive boundaries in the TLM model," in *Proc. Int. Conf. Comput. Electromagnetics,* London, Dec. 1991, pp. 67–70.

[10] Meliani, D. de Cogan, and P. B. Johns, "The use of orthogonal curvilinear meshes in TLM models," *Int. J. Numerical Modeling,* vol. 1, pp. 221–238, 1988.

[11] P. B. Johns, "A symmetrical condensed node for the TLM method," *IEEE Trans. Microwave Theory Tech.,* vol. 35, pp. 370–377, Apr. 1987.

[12] P. Naylor and R. A. Desai, "New three dimensional symmetrical condensed lossy node for solution of electromagnetic wave problems by TLM," *Elec. Lett.,* vol. 26, pp. 492–494, 29th March 1990.

[13] M. Abramowitz and I. A. Stegun, *Handbook of Mathematical Functions.* New York: Dover, p. 635, 1965.

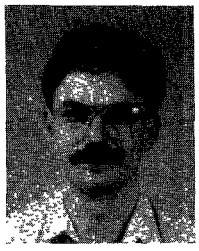

Ian G. Gosling was born in Hitchin, England, in 1955. He received the B.A. degree in natural sciences (physics) in 1977, and the M.A. and Ph.D. degrees in microwave engineering in 1981, all from the University of Cambridge, England. His doctoral thesis was on the subject of microwave cavity design for high power gyrotron oscillators.

In 1981, he joined British Telecom Research Laboratories, working on millimetre-wave integrated circuits, monolithic circuits and test systems, and computer-aided design. In 1988, he was appointed as a Senior Lecturer in the Centre for Networking Research, School of Electrical Engineering, Nanyang Technological University, Singapore.

Dr. Gosling has published at least 20 papers and patents. His current research interests include computer-aided modeling of microwave components and communications systems.